

# Transport Simulation of PLATO Tokamak Plasma Using Integrated Code TASK

Shota MOCHINAGA<sup>1)</sup>, Naohiro KASUYA<sup>1,2)</sup>, Atsushi FUKUYAMA<sup>3)</sup>,  
Yoshihiko NAGASHIMA<sup>1,2)</sup> and Akihide FUJISAWA<sup>1,2)</sup>

<sup>1)</sup>*Interdisciplinary Graduate School of Engineering Sciences, Kyushu University, Kasuga, Fukuoka 816-8580, Japan*

<sup>2)</sup>*Research Institute for Applied Mechanics, Kyushu University, Kasuga, Fukuoka 816-8580, Japan*

<sup>3)</sup>*Kyoto University, Nishikyo-ku, Kyoto 615-8540, Japan*

(Received 16 February 2021 / Accepted 7 June 2021)

Transport simulations using the integrated code TASK are performed on the PLATO tokamak to forecast plasma performance. For transport simulations considering the experimental conditions, MHD equilibria are obtained by taking into account the external coil current condition. Dependences of the plasma parameters on externally controllable quantities in the experiment, such as the amount of particle fuel and values of the external coil currents, exhibit an increase on the order of 10% in the ion temperature without direct ion heating.

© 2021 The Japan Society of Plasma Science and Nuclear Fusion Research

Keywords: transport simulation, integrated simulation code, PLATO, tokamak, power balance

DOI: 10.1585/pfr.16.1403093

## 1. Introduction

PLATO at Kyushu University is a tokamak device used to observe detailed spatiotemporal structures in plasma turbulence with several diagnostic tools, such as tomography systems with more than 1500 detectors and three heavy ion beam probes [1, 2]. The interaction between multiple instabilities is one of the targets for the observations. PLATO is a rather small tokamak (plasma major radius:  $R = 0.7$  m; plasma minor radius:  $a = 0.2$  m), and only ohmic heating is used for plasma heating. There is no external heating mechanism for ions in the first phase of the PLATO experiment; thus, finding ways to increase the ion temperature is a problem that needs to be addressed as the ion temperature is important for observing ITG turbulence. Increasing the energy exchange from electrons to ions and enhancing the plasma confinement are two possible strategies for increasing the ion temperature. The particle supply control, which is related to the magnitude of the collisionality between ions and electrons, and the plasma shape control, which is related to the confinement, are among the external controls already applicable during an experimental discharge. Quantitative evaluations obtained through simulations are necessary. Since the plasma performance is determined through the multiple physical processes of the plasma equilibrium, transport, heating, etc., integrated transport simulations are useful to forecast the temperature in the PLATO plasma parameter region. For the performance evaluation of tokamak plasmas, many integrated codes have been developed [3–6]. In this study, we perform 1.5-dimensional (1.5D) transport simulations of the PLATO plasma using the integrated code TASK.

The TASK code has been used to simulate the core plasma transport and analyze heating via RF and NBI [7, 8]. Conventional transport analyses with the TASK code have been conducted through the combination of a fixed-boundary two-dimensional (2D) equilibrium module, TASK/EQ, and a one-dimensional (1D) transport module, TASK/TR. The fixed-boundary module only calculates the equilibrium inside the last-closed flux surface. The confined plasma shape in tokamaks is determined by the magnetic configuration generated by the plasma current and the external coil currents. Therefore, to evaluate the effect of the control on the plasma shape, a free-boundary calculation of equilibria is necessary to obtain the equilibrium condition, taking the external coil conditions into account. For this reason, in this study, we developed a data-transfer interface in the TASK code to include the free-boundary 2D equilibrium module TASK/EQU, which calculates the plasma equilibrium, taking into account the vertical field coils. This addition has made it possible to evaluate the dependence of the plasma performance on the plasma volume under realistic conditions. The TASK/EQU module has also been used for the calculations of the MHD instabilities in PLATO [9].

In this work, we explain the results obtained from transport simulations using the developed TASK code to evaluate how much the ion temperature is expected to increase by changing controllable parameters in PLATO. The combinations of the transport processes are quantitatively clarified from the evaluation of the power balance in the steady state.

author's e-mail: mochinaga@riam.kyushu-u.ac.jp

## 2. Transport Simulation Model

For transport simulations with the actual magnetic configuration in tokamak devices, we have developed a 1.5D transport simulation scheme linking the 2D TASK/EQU equilibrium module with the 1D TASK/TR transport module. The metrics evaluated in the 2D equilibrium, which takes the external coil conditions into account, are transferred to the transport module through the BPSD data interface. The plasma profiles obtained via the transport simulations are also transferred to the equilibrium module. In the equilibrium calculation, the following Grad–Shafranov equation is solved:

$$\nabla \frac{1}{R^2} \nabla \psi = -4\pi^2 \mu_0 \frac{dp}{d\psi} - \frac{I}{R^2} \frac{dI}{d\psi}. \quad (1)$$

Here,  $\psi$ ,  $p$ ,  $I$ ,  $R$ , and  $\mu_0$  denote the poloidal flux function, plasma pressure, poloidal current, major radius, and permeability, respectively. In the free-boundary equilibrium calculation in TASK/EQU,  $\psi$  includes contributions from both the plasma current  $\psi_p$  and the external vertical coil current  $\psi_{coil}^i$  according to  $\psi = \psi_p + \sum_i \psi_{coil}^i$ , where  $i$  denotes the index number of the coils. In the equilibrium calculation linked to the transport calculation, the pressure profile obtained from the transport calculation is used as an initial condition, and the poloidal current profile is derived from the safety factor  $q$  in the right-hand side of Eq. (1). In this study, the change in the current profile on the flat top of the plasma discharges is considered to be small and is not reconstructed in the evolution.

In the transport calculation, the following particle and heat transport equations are solved for  $s$  plasma species:

$$\frac{1}{V'} \frac{\partial}{\partial t} (n_s V') = -\frac{1}{V'} \frac{\partial (V' \Gamma_s)}{\partial \rho} + S_s, \quad (2)$$

$$\frac{1}{V'^{5/3}} \frac{\partial}{\partial t} \left( \frac{3}{2} n_s T_s V'^{5/3} \right) = -\frac{1}{V'} \frac{\partial (V' Q_s)}{\partial \rho} + P_s. \quad (3)$$

Here,  $n_s$ ,  $T_s$ ,  $S_s$ ,  $P_s$ , and  $\rho$  denote the plasma density, plasma temperature, particle source, heat source, and normalized minor radius, respectively, and  $V' = dV/d\rho$  denotes the radial derivative of the plasma volume. Assuming particle supply by gas puffing, the electron and ion sources are given by the following equation:

$$S_s = S_0 \exp \left[ -\left( \frac{r-r_0}{r_w} \right)^2 \right], \quad (4)$$

where  $S_0$  denotes the intensity of the particle fueling, and the function shape is defined by the radial position  $r_0$  and radial width  $r_w$ . The heat sources for electrons and ions are given by

$$P_e = P_{OH} - P_{EQ}, \quad (5)$$

$$P_i = P_{EQ}, \quad (6)$$

where  $P_{OH}$  denotes the ohmic heating power expressed as follows:

$$P_{OH} = \eta j^2, \quad (7)$$

and  $P_{EQ}$  is the collisional energy transfer from electrons to ions expressed as follows:

$$P_{EQ} = \frac{3}{2} n \frac{T_e - T_i}{\tau_{ei}}. \quad (8)$$

Here,  $\eta$  denotes the plasma resistivity,  $j$  denotes the plasma current density, and

$$\tau_{ei} = \frac{3 \sqrt{2} \pi^{1.5} \epsilon_0^2 m_e m_i}{n e^4 Z_e Z_i \ln \Lambda} \left( \frac{T_e}{m_e} + \frac{T_i}{m_i} \right)^{1.5}, \quad (9)$$

is the electron-ion collision time. The particle flux  $\Gamma_s$  and heat flux  $Q_s$  are given by the following equation:

$$\Gamma_s = \langle |\nabla \rho| \rangle V_s n_s - \langle |\nabla \rho|^2 \rangle D_s \frac{\partial n_s}{\partial \rho}, \quad (10)$$

$$Q_s = \langle |\nabla \rho| \rangle \frac{3}{2} n_s T_s V_{Es} - \langle |\nabla \rho|^2 \rangle n_s \chi_s \frac{\partial T_s}{\partial \rho} + \frac{3}{2} \Gamma_s T_s, \quad (11)$$

where  $V_s$  denotes the particle pinch velocity;  $D_s$ , the particle diffusivity;  $V_{Es}$ , the heat pinch velocity;  $\chi_s$ , the thermal diffusivity; and  $\langle \rangle$ , a magnetic flux surface average. Quantities regarding the plasma shape, metric, and magnetic-surface averages are obtained from the equilibrium calculations to yield  $V'$ ,  $\langle |\nabla \rho| \rangle$ , and  $\langle |\nabla \rho|^2 \rangle$  in the transport equations. In the particle transport equation, the quasi-neutrality condition is assumed. Transport coefficients include neoclassical and turbulent contributions. For the neoclassical transport model, the NCLASS module [10] is utilized to obtain the diffusion coefficients and convection velocities of particles and heat. The plasma resistivity is also obtained using the NCLASS module. For turbulent transport, the CDBM model [11] is utilized to obtain the thermal diffusivity, which is expressed as follows [12]:

$$\chi_{CDBM} = F(s, \alpha, \kappa) \alpha^{\frac{3}{2}} \frac{c^2}{\omega_{pe}^2} \frac{v_A}{qR}, \quad (12)$$

where,  $c$  denotes the speed of light;  $\omega_{pe}$ , the electron plasma frequency;  $v_A$ , the Alfvén velocity;  $q$ , the safety factor;  $s \equiv (r/q)(dq/dr)$ , the magnetic shear;  $\alpha \equiv -(2\mu_0 q^2 R/B^2)(dp/dr)$ , the normalized pressure gradient; and  $\kappa \equiv -(r/R)(1 - q^{-2})$ , the magnetic curvature. The factor  $F(s, \alpha, \kappa)$  is represented as a function of  $s - \alpha$  with approximation for  $q > 1$ . The stabilizing effect of the  $E \times B$  flow shear is not considered in this study. The transport coefficients are the sum of the neoclassical and turbulent thermal diffusion coefficients according to the following

$$\chi_s = \chi_{s,NCLASS} + C \chi_{CDBM}, \quad (13)$$

where,  $C = 12.0$ , which is the correction between the CDBM confinement time and the  $\tau_{89}^{ITER}$  confinement scaling.

By exchanging data between the equilibrium and transport calculation modules, the time evolutions of the plasma quantities are solved with the TASK/TOT time evolution control module.

### 3. Transport Simulation with PLATO Parameter

The developed scheme (EQU–TR combination) that includes the models presented in the previous section is used to forecast plasma performances and transport properties with the PLATO plasma parameters. The toroidal magnetic field ( $B_t$ ) and plasma current ( $I_p$ ) were kept constant at 0.3 T and 40 kA. The PLATO device has three main pairs of vertical field coils, namely dipole (D), quadrupole (Q), and hexapole (H) coils, and two pairs of feedback coils, the F1 and F2 coils, as presented in Fig. 1. The ohmic heating coil in the center solenoid is divided into two pairs, namely, the OH and OHC coils [13]. In this calculation, only the D, Q, and H coils are considered for control, and the following coil currents are used:

OH/OHC coils	: -67.2 kA turn,
D coils	: -23.3 kA turn,
Q coils	: +38.4 kA turn,
H coils	: -10.8 kA turn,

where the values are positive when the direction of the current is the same as that of the plasma current. Figure 1 presents the poloidal cross section of the flux contours of the equilibrium condition in the case of the EQU calculation. The obtained equilibrium is characterized by  $R = 0.7$  m,  $a = 0.18$  m, an ellipticity ( $\kappa$ ) of 1.9, and a triangularity ( $\delta$ ) of 0.4. The density at the magnetic axis is set to  $n_0 = 1.0 \times 10^{19} \text{ m}^{-3}$  by fueling electrons and hydrogen ions by the particle source terms in Fig. 2 (a). The gas-puffing method is the main particle supply in PLATO; thus, this time-constant source profile is assumed to peak near the plasma edge at  $\rho = 0.7$ . The plasma profiles in the steady state are obtained as in Fig. 2 (Case A). The electron and ion temperatures are  $T_{e,0} = 130 \text{ eV}$  and  $T_{i,0} = 35 \text{ eV}$ , re-

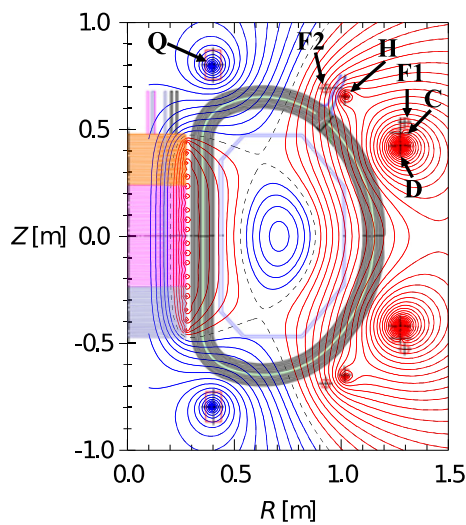


Fig. 1 Equilibrium magnetic configuration of the PLATO tokamak obtained using the TASK/EQU module. The respective positions of the vertical field coils and ohmic coils are also shown.

spectively, at the magnetic axis; therefore,  $T_{i,0}$  is less than  $T_{e,0}/3$ . There is no direct ion heat source; hence, the ion temperature is determined by the competition between the energy transfer from electrons and the heat fluxes. As presented in Fig. 2 (e), the neoclassical convection is directed inward, but the diffusion contribution is much larger. The turbulent diffusion is dominant with the exception of close to the magnetic axis, where the density and temperature profiles are rather flat, as presented in Fig. 2 (f).

For the comparison, the conventional transport analysis method (EQ–TR combination) is also employed using the same shaping parameters. Similar results are obtained with EQ and EQU, but the electron temperature in the EQU–TR case is higher than that in the EQ–TR case as the ohmic heating power is different, as presented in Fig. 2 (d). In the EQU–TR case, the current is larger near the magnetic axis for the same total plasma current.

### 4. Particle Fueling Rate Control

A large difference between  $T_i$  and  $T_e$ , similar to that observed in the previous section, is expected in PLATO; thus, evaluations are made with regard to how much  $T_i$  can be increased. One possibility is that of increasing the energy transfer from the electrons, which depends on the density. Transport simulations are performed in the PLATO plasma parameter region to obtain the density dependence by changing the particle fueling rate. Here, the plasma pa-

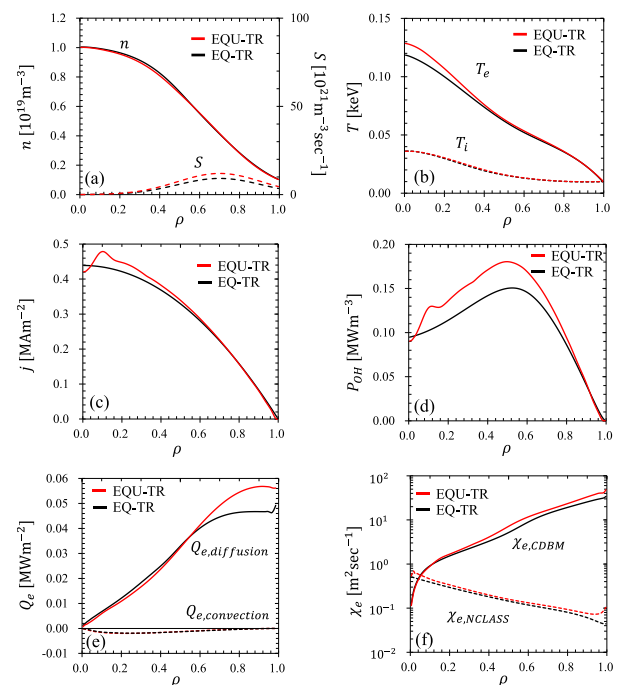


Fig. 2 Radial profiles of (a) the density and particle source, (b) electron and ion temperatures, (c) current density, (d) ohmic heating power, (e) electron heat flux, (f) electron thermal diffusivity. The cases for EQU–TR and EQ–TR are shown.

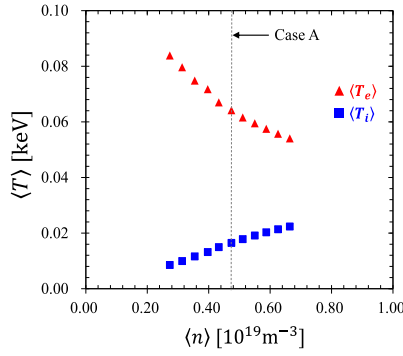


Fig. 3 Relation between the volume-averaged temperature and density, when the particle fueling rate is changed.

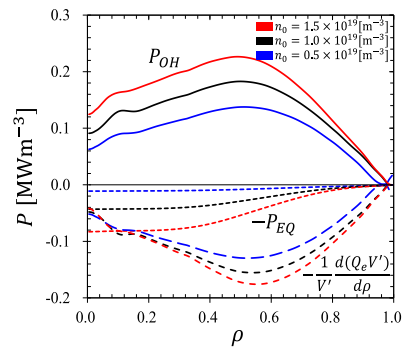


Fig. 4 Radial profiles of the ohmic power, equipartition power and electron heat transport term. The cases with  $n_0 = 0.5, 1.0$  and  $1.5 \times 10^{19} \text{ m}^{-3}$  are shown.

rameters and coil currents are set to be the same as those in the previous section. The intensity of the particle fueling is adjusted from  $S_0 = 6.0$  to  $17.7 \times 10^{21} \text{ m}^{-3} \text{ sec}^{-1}$  to increase the density at the magnetic axis from  $n_0 = 0.5$  to  $1.5 \times 10^{19} \text{ m}^{-3}$ . The particle transport demonstrates that  $n_0$  is almost proportional to  $S_0$ . Figure 3 indicates that the electron temperature decreases as  $\langle T_e \rangle \propto \langle n \rangle^{-0.5}$ , and the ion temperature increases as  $\langle T_i \rangle \propto \langle n \rangle^{1.1}$ , in accordance with the density increase. The ion temperature can be increased to  $T_{i,0} = 45 \text{ eV}$  with  $\langle n \rangle = 0.66 \times 10^{19} \text{ m}^{-3}$ , thus, it is 30% higher than that in case A with  $\langle n \rangle = 0.47 \times 10^{19} \text{ m}^{-3}$ . This temperature can be explained in terms of the power balance between electrons and ions. As can be seen from Eq. (3), the power balance is satisfied when the ohmic heating power, energy transfer from electrons to ions and heat fluxes in the steady state obey the following relationships:

$$\text{Electron} \quad : \quad -\frac{1}{V'} \frac{\partial(V'Q_e)}{\partial\rho} + P_{OH} - P_{EQ} = 0, \quad (14a)$$

$$\text{Ion} \quad : \quad -\frac{1}{V'} \frac{\partial(V'Q_i)}{\partial\rho} + P_{EQ} = 0. \quad (14b)$$

Figure 4 presents the radial profiles of the three terms in Eq. (14a) with  $n_0 = 0.5, 1.0$ , and  $1.5 \times 10^{19} \text{ m}^{-3}$ , and the

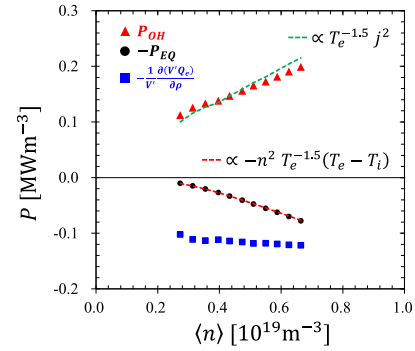


Fig. 5 Density dependence of the terms in Eq. (14a) at  $\rho = 0.3$ , which satisfies the power balance condition.

values at  $\rho = 0.3$ , where the temperature gradient is large, are selected in Fig. 5 for the explanation. These results satisfy Eq. (14a). A larger density leads to an increase in the electron flux and  $P_{EQ}$ . Equations (8) and (9) give

$$P_{EQ} \propto n^2 T_e^{-1.5} (T_e - T_i). \quad (15)$$

The electron-ion collision is responsible for the energy exchange between electrons and ions, which makes the temperature difference between electrons and ions smaller. The increases in  $n^2$  and  $T_e^{-1.5}$  and the decrease in  $(T_e - T_i)$  determine the magnitude of  $P_{EQ}$ , as indicated by the red dashed line in Fig. 5. Including the dependence on temperature, the density dependence is  $P_{EQ} \propto n^{1.8}$ . Therefore, the ion temperature increases, as  $P_{EQ}$  increases. In addition, the larger plasma resistivity results in a  $P_{OH}$  increase. Equation (7) and the plasma resistivity

$$\eta \propto \frac{m_e}{ne^2\tau_{ei}}, \quad (16)$$

give the following relation:

$$P_{OH} \propto T_e^{-1.5} j^2. \quad (17)$$

The deviation from this relation indicated by the green dashed line in Fig. 5 results from the density dependence of the neoclassical resistivity determined by the NCLASS routine. Despite the change in  $P_{OH}$ , a larger density leads to an increase in the electron flux and  $P_{EQ}$ , which results in a lower electron temperature.

## 5. Coil Current Control

The second transport calculation is performed with variation of an external coil current. The plasma shape is related to the plasma confinement; therefore, the dependence on the plasma volume  $V_p$  is investigated by changing the external coil currents. The D-coil current is changed in the range from  $-18.8$  to  $-23.3 \text{ kA turn}$ , whereas the other plasma parameters and coil currents are previous sections. The intensity of the particle fueling is set to yield the constant total particle fueling rate  $\int S dV_p$ . The equilibrium

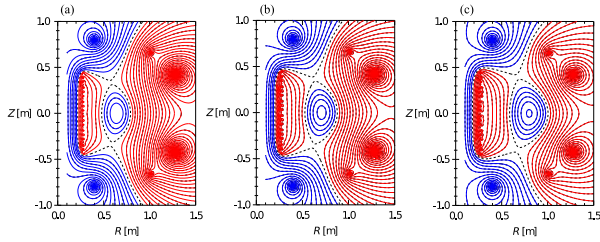


Fig. 6 Equilibrium magnetic configurations with D-coil current of (a)  $-28.8$ , (b)  $-23.3$ , and (c)  $-18.8$  kA turn.

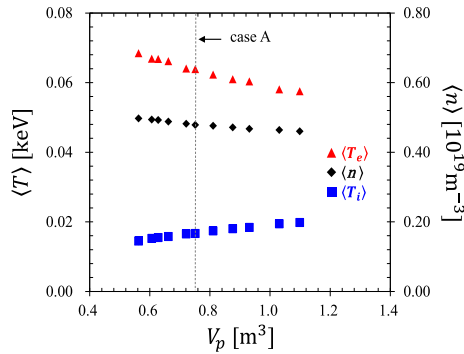


Fig. 7 Relation between the volume-averaged density, ion and electron temperatures and the plasma volume. This is the case when the D-coil current is changed.

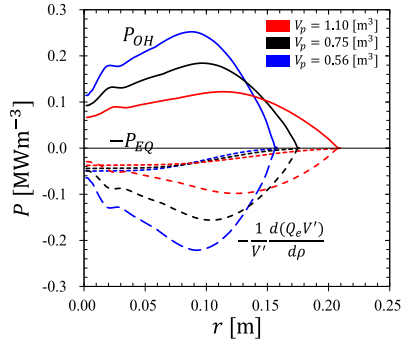


Fig. 8 Radial profiles of the ohmic power, equipartition power and electron heat transport term.

magnetic configuration is changed as in Fig. 6. In the transport model in the TR module, the effect of the plasma shape is introduced by the plasma volume, metric  $\langle |\nabla\rho|^2 \rangle$  and  $\langle |\nabla\rho|^2 \rangle$ . As can be seen from Fig. 7, the density slightly decreases with the increase in the plasma volume. The particle source  $S(r)$  decreases, whereas the total particle fueling rate remains constant; however, the density the same as those in the variation is limited due to the decrease in the particle fluxes. Conversely, the larger the plasma size, the lower the electron temperature, and the higher the ion temperature.

The ion temperature is increased to  $T_{i,0} = 41$  eV for  $V_p = 1.10$  m<sup>3</sup>; therefore, it is 15% higher than that in case

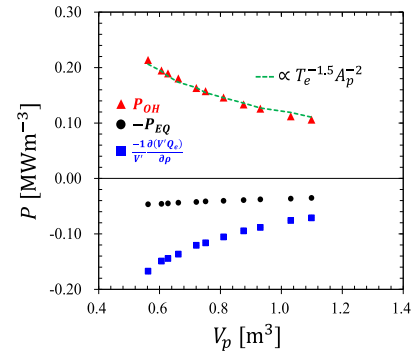


Fig. 9 Plasma volume dependence of the terms in Eq. (14a) at  $\rho = 0.3$ .

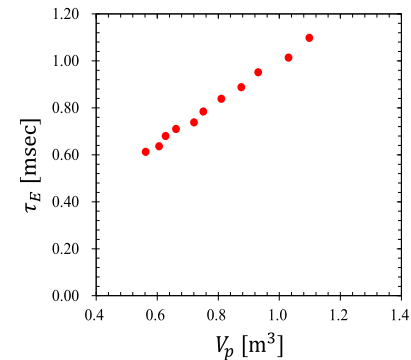


Fig. 10 Plasma volume dependence of the energy confinement time.

A with  $V_p = 0.75$  m<sup>3</sup>.

The temperature change can be explained in terms of the power balance. Figure 8 presents the radial profiles of the terms in the power balance of the electrons. The values at  $\rho = 0.3$  are also selected in Fig. 9 for explanation of this dependence. Since the plasma current is kept constant, the current density decreases in accordance with the increase in the plasma volume. The ohmic power  $P_{OH}$  is expressed as follows:

$$P_{OH} \propto T_e^{-1.5} A_p^{-2}, \quad (18)$$

where  $A_p$  denotes the size of the plasma poloidal cross-section, and  $V_p \approx 2\pi R A_p$ . Therefore,  $P_{OH}$  decreases depending on  $A_p$ , as can be seen from Fig. 9, which results in a decrease in the electron temperature.  $P_{EQ}$  slightly decreases due to the small density decrease as  $A_p$  increases, but the energy confinement time increases (Fig. 10) as a result of the small change in the thermal diffusivity and the increase in the plasma minor radius. Therefore, the ion temperature increases due to the improvement of confinement.

## 6. Conclusions

In this study, the transport simulations were conducted using free-boundary condition equilibria, considering the

external vertical field coils in the PLATO experiments. The plasma performance was forecasted in PLATO. The dependence of the plasma performance on the particle fuelling rate and vertical field coil current, which are externally controllable parameters in the experiments, were evaluated for the estimation of the ion temperature. A temperature increase was forecasted from these two different methods, namely, changing the energy transfer from electrons to ions, and the energy confinement time. In the initial phase of the PLATO experiments, there is no direct ion heating method; therefore, these indirect methods represent possible strategies to increase the ion temperature. Conversely, the electron temperature is decreased; thus, appropriate plasma parameters must be selected to obtain the optimum conditions.

In the present code, the toroidal current profiles obtained via the transport calculation are not taken into account in the equilibrium calculation; thus, it is necessary to introduce the data-transfer process for self-consistent calculations. In addition, the transport prediction accuracy will be improved through comparisons with experimental results in future works.

## Acknowledgments

This study was partially supported by the Grant-in-

Aid for Scientific Research (JP16K06938, JP17H06089, JP20K03905) of JSPS and by the collaboration program of NIFS (NIFS19KNST144), QST (on development research of the fusion DEMO reactor), and RIAM of Kyushu University.

- [1] A. Fujisawa, AIP Conf. Proc. **1993**, 020011 (2018).
- [2] T. Ido *et al.*, Rev. Sci. Instrum. (2021) in press.
- [3] N. Hayashi and JT-60 Team, Phys. Plasmas **17**, 056112 (2010).
- [4] Y. Murakami *et al.*, J. Nucl. Mater. **313-316**, 1161 (2003).
- [5] V. Parail *et al.*, Nucl. Fusion **49**, 075030 (2009).
- [6] G. Giruzzi *et al.*, Nucl. Fusion **55**, 073002 (2015).
- [7] M. Honda *et al.*, J. Plasma Fusion Res. SERIES **6**, 160 (2004).
- [8] H. Nuga *et al.*, Prog. Nucl. Sci. Technol. **2**, 78 (2011).
- [9] S. Tomimatsu *et al.*, Plasma Fusion Res. **15**, 1403052 (2020).
- [10] W. Houlberg *et al.*, Phys. Plasmas **4**, 3230 (1997).
- [11] M. Yagi *et al.*, Phys. Fluids B **5**, 3702 (1993).
- [12] A. Fukuyama *et al.*, Plasma Phys. Control. Fusion **37**, 611 (1995).
- [13] K. Matsuoka, RIAM Reports, Kyushu Univ. **141**, 51 (2011) (in Japanese).